ADVANCED FUNCTIONAL MATERIALS

www.afm-journal.de

Plant-Based Hollow Microcapsules for Oral Delivery Applications: Toward Optimized Loading and Controlled Release

Michael G. Potroz, Raghavendra C. Mundargi, Jurriaan J. Gillissen, Ee-Lin Tan, Sigalit Meker, Jae H. Park, Haram Jung, Soohyun Park, Daeho Cho, Sa-Ik Bang, and Nam-Joon Cho**

Efficient oral administration of protein-based therapeutics faces significant challenges due to degradation from the highly acidic conditions present in the stomach and proteases present in the digestive tract. Herein, investigations into spike-covered sunflower sporopollenin exine capsules (SECs) for oral protein delivery using bovine serum albumin (BSA) as a model drug are reported and provide significant insights into the optimization of SEC extraction, SEC loading, and controlled release. The phosphoric-acid-based SEC extraction process is optimized. Compound loading is shown to be driven by the evacuation of air bubbles from SEC cavities through the porous SEC shell wall, and vacuum loading is shown to be the optimal loading method. Three initial BSA-loading proportions are evaluated, leading to a practical loading efficiency of 22.3 ± 1.5 wt% and the determination that the theoretical maximum loading is 46.4 ± 2.5 wt%. Finally, an oral delivery formulation for targeted intestinal delivery is developed by tableting BSA-loaded SECs and enteric coating. BSA release is inhibited for 2 h in simulated gastric conditions followed by 100% release within 8 h in simulated intestinal conditions. Collectively, these results indicate that sunflower SECs provide a versatile platform for the oral delivery of therapeutics.

1. Introduction

The microencapsulation of drugs has been extensively studied over the past few decades, and major achievements had been made; nevertheless, a long-standing, remaining challenge is the rapid and low-cost manufacturing of microcapsules with uniform size, porosity, and architecture, particularly for oral delivery of therapeutic proteins.[1,2] Sporopollenin exine capsules (SECs), which are extracted from natural pollen, provide an attractive, natural, and robust drug delivery system due to their striking structural uniformity, mechanical and chemical robustness, monodisperse size and porosity, large inner cavity, and abundant availability. In nature, sporopollenin forms the outermost layer of pollen grains and is responsible for the safe and protective transportation of the enclosed reproductive genetic materials under diverse environmental conditions.[3,4] Moreover, pollen and SECs have been explored for their nutritional and therapeutic effects, as well as the encapsulation of drugs, proteins, vaccines, and oils.[4–12] These features and particularly the SECs' inherent physicochemical robustness make them an excellent candidate for encapsulating therapeutic proteins for oral delivery with controlled release.[3,4,7,8]

In recent years, therapeutic proteins have emerged as an important treatment option, and they represent a massive

M. G. Potroz, Dr. R. C. Mundargi, Dr. J. J. Gillissen, E.-L. Tan, Dr. S. Meker, J. H. Park, H. Jung, S. Park, Prof. N.-J. Cho
School of Materials Science and Engineering
Nanyang Technological University
50 Nanyang Avenue, 639798 Singapore, Singapore
E-mail: njcho@ntu.edu.sg

M. G. Potroz, Dr. R. C. Mundargi, Dr. J. J. Gillissen, E.-L. Tan, Dr. S. Meker, J. H. Park, H. Jung, S. Park, Prof. N.-J. Cho
Centre for Biomimetic Sensor Science
Nanyang Technological University
50 Nanyang Drive, 637553 Singapore, Singapore

Prof. D. Cho
Department of Cosmetic Sciences
Sookmyung Women's University
Yongsan-ku, Seoul 140-742, Republic of Korea

Prof. S.-I. Bang
Department of Plastic Surgery
Samsung Medical Center
Sungkyunkwan University School of Medicine
50 Ilwon-dong, Gangnam-gu, Seoul 135-710, Republic of Korea
E-mail: si55.bang@samsung.com

Prof. N.-J. Cho
School of Chemical and Biomedical Engineering
Nanyang Technological University
62 Nanyang Drive, 637459 Singapore, Singapore

DOI: 10.1002/adfm.201700270

share of the pharmaceutics market.[13–17] The administration of therapeutic proteins largely involves injections,[14,18] which suffer from low patient compliance and are often painful;[2,19] on the other hand, oral delivery is a convenient and painless administration route and is preferred by patients.[2,18] Nevertheless, due to the harsh environment of the stomach, only negligible amounts of unprotected therapeutic proteins typically reach the intended delivery site, and the oral delivery of proteins is therefore limited.[2,18,20–22] Various delivery systems have been explored to overcome this challenge, including the use of copolymers as an enteric coating.[13,19,22–25] In particular, enteric coating using a copolymer of methacrylic acid and methyl methacrylate (Eudragit), which is insoluble in acidic pH, has been shown to provide protection in low pH conditions.[25] Although progress has been made, oral delivery of proteins is still lacking a cost effective and efficient encapsulation process.[2,20]

So far, SECs have been explored for the encapsulation of proteins and it is suggested that their mechanical and chemical durability may facilitate the oral delivery of proteins.[5,26,27] Interestingly, enzymes encapsulated into *Lycopodium clavatum* SECs have been shown to retain their functionality following their release from the SECs, thus implying the protective nature of SECs toward encapsulated proteins.[5] Sporopollenin is a complex biopolymer, which forms the outer shell structure of SECs, and is known to exhibit morphological stability under harsh chemical processing, such as acetolysis, acidolysis, and exposure to solvents. Recently, we introduced an ecofriendly streamlined extraction process for obtaining SECs from natural (*L. clavatum*) spores and natural sunflower (*Helianthus annuus*) pollen grains while retaining their unique microstructure;[3,28] thus contributing to the potential of using pollen as the basis of a cost-effective microencapsulation system.

Herein, we expand on the potential of SECs for drug delivery applications by conducting the optimization of SEC extraction, SEC loading, and controlled release. Our results provide significant insights into the mechanisms and potential of compound loading and drug delivery utilizing SECs or other porous microcapsule systems. Initially, the efficiency of the SEC extraction process was improved and the SECs were characterized in different stages of the encapsulation and tableting processes to study their morphological stability. The loading kinetics were characterized, and key factors affecting the loading process were identified. Insights that were gained from mechanistic evaluation were then applied to explore the practical and theoretical potential of compound loading. Finally, we demonstrate that tableted bovine serum albumin (BSA)-loaded SECs with an enteric coating (Eudragit L100) provide an effective method for the oral delivery of therapeutic proteins. Overall, the schematic diagram in **Figure 1** outlines the transition of sunflower pollen into SECs, BSA loading into SECs, and tableting with enteric coating for intestinal protein delivery.

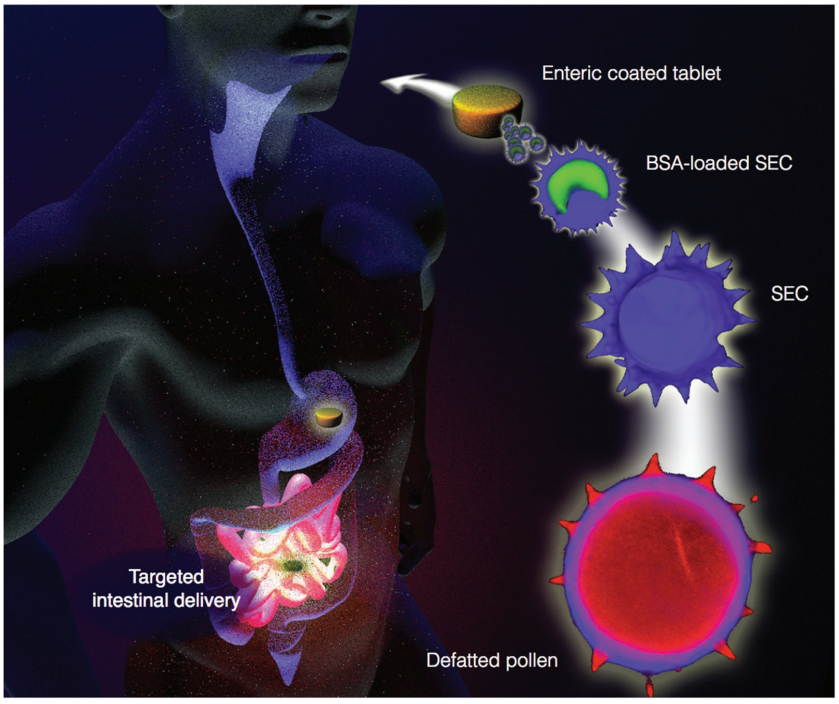

Figure 1. Schematic diagram showing the development of tableted sporopollenin exine capsules for intestinal protein delivery.

2. Results and Discussion

2.1. SEC Extraction Optimization and Analysis

We have previously reported the extraction process of intact sunflower pollen SECs.[28] In continuation, we have optimized the SEC extraction by conducting acidolysis with phosphoric acid (85% v/v) at four different durations, 1, 5, 10, and 20 h. To improve the efficiency of the process, it is important to remove the cytoplasmic contents from the inner cavity in the minimum time possible, while maintaining the intactness of the SECs. Comprehensive SEM analysis indicated that all acidolysis treatment durations produced a clean inner cavity and intact external microstructure (**Figure 2**; Figure S1, Supporting Information). Confocal laser scanning microscopy (CLSM) analysis also showed that H_3PO_4 acidolysis achieved effective removal of internal cytoplasmic contents, indicated by an absence of autofluorescence in the internal cavity following acidolysis processing (Figure 2; Figure S2, Supporting Information). The reduced size of processed SECs is attributed to the removal of sunflower pollen cytoplasmic constituents (SEM or CLSM).[28] The efficacy of protein removal was also characterized by elemental (CHN) analysis; the quantity of nitrogen in plant materials is assumed to be proportional to protein content.[3–5,7–9,28] A comparative analysis of the protein removal efficacy, based on % nitrogen content, indicated that 5 h of H_3PO_4 treatment resulted in the maximum possible protein removal (Figure 2A; Figure S3 and Table S1, Supporting Information).

Acid hydrolysis of proteins is common in food processing to produce acid protein hydrolysates. Medium temperature, short duration, strong acid processing produces peptides from proteins,

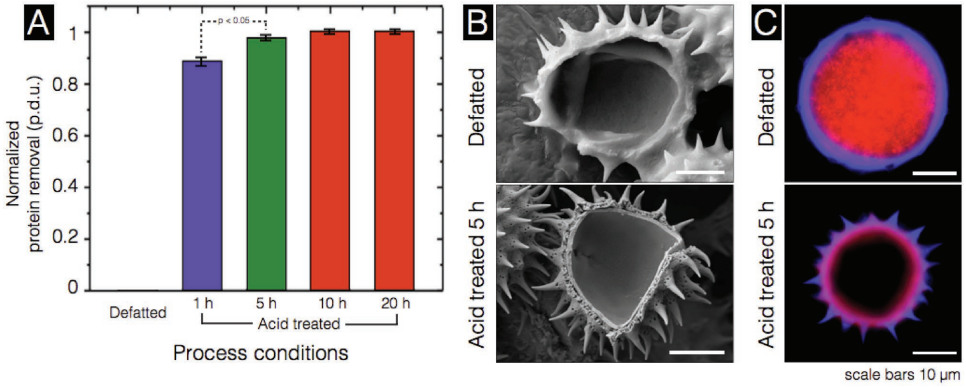

Figure 2. Optimized sunflower pollen sporopollenin exine capsule (SEC) extraction: A) Comparative analysis of protein removal efficacy following H_3PO_4 acidolysis, based on % nitrogen content; data are presented as the average of triplicate measurements with standard deviation (n = 3); B) Scanning electron microscope cross-sectional images of a defatted sunflower pollen grain and SEC following 5 h H_3PO_4 acidolysis; and C) Confocal microscopy analysis of a defatted sunflower pollen grain and SEC following 5 h H_3PO_4 acidolysis.

which are typically in the 1 to 20 kDa range.[29] Mass spectrometry, matrix-assisted laser desorption/ionization-time of flight (MALDI-TOF), was performed with ground and ethanol extracted samples. Analysis of defatted pollen indicated multiple peaks present in the 2500 to 4500 m/z range, suggesting the presence of large biomacromolecules. However, these peaks were absent in all of the 1, 5, 10, and 20 h acid-processed SECs (Figure S4, Supporting Information), supporting the effective removal of proteinaceous compounds as observed by elemental analysis.

For morphological analysis, the size of sunflower pollen grains was characterized by dynamic imaging particle analysis (DIPA) (Figure S5, Supporting Information) following different acidolysis durations. DIPA data imply that the SEC extraction resulted in the reduction of intact particle diameter, from 37.0 ± 1.5 µm for natural pollen grains to 30.3 ± 0.9 µm for 5, 10, and 20 h processed SECs (Figure S5 and Table S2, Supporting Information), respectively. This supports the reduction in particle size observed by other techniques including SEM and CLSM. Moreover, the micromeritic analysis regarding circularity and aspect ratio of SECs processed at different periods exhibited a near to circular shape with no significant difference between processed SECs and native pollen (Figure S5, Supporting Information). The DIPA analysis indicates uniform morphology and intactness of SEC architecture in comparison to native pollen grains (Figure S6, Supporting Information). Overall, based on the intactness of the pollen microstructure, the cleanliness of the internal cavity, and the efficacy of proteinaceous nitrogen removal, it was determined that 5 h H_3PO_4-treated SECs would be used in the remainder of this study.

2.2. Mechanistic Evaluation of Protein Loading

To ensure an industrially applicable loading protocol, it is important to achieve optimal loading with minimal processing requirements. However, due to the limited quantity of literature regarding SECs for use in microencapsulation, there is limited understanding regarding the fundamental loading mechanisms of these porous microcapsules. Therefore, the initial goal was to determine how it is possible to completely fill all SECs with the loading solution, and then to understand the processes driving complete loading.

To explore the loading phenomenon, we performed CLSM analysis of SECs loaded by modified passive loading, vortex mixing, and vacuum loading methods so as to retain the SECs in an aqueous fluorescein isothiocyanate-conjugated BSA (FITC–BSA) solution environment (**Figure 3**). Passive loading was performed by real-time CLSM imaging of SECs submerged in FITC–BSA solution for up to 60 min, whereas vortex mixed and vacuum loaded samples were analyzed after processing. Passive loading observations indicated that overall FITC–BSA loading inside SEC cavities increases with time. Interestingly, a time lag prior to the loading of most SECs was detected; this is attributed to the surface tension existing between air pockets within the SECs and the FITC–BSA solution. Additionally, a significant proportion of SECs was not loaded, even after 60 min. CLSM analysis revealed that once an SEC began to load, full SEC loading was achieved in ≈15 min. Loading assisted by vortex mixing improved the loading efficacy, compared with passive loading; nonetheless, the application of a vacuum was necessary for complete particle loading. The observed loading of FITC–BSA solution under vacuum may be attributed to the creation of a negative pressure differential occurring when the air is evacuated from the inner cavity of the SECs.[3,4] Based on our mechanistic loading observations, we proceeded with vacuum loading for the remainder of the study.

However, to further clarify the forces driving loading, a mathematical model for liquid loading into SECs was derived (Experimental Section: *BSA Loading into Sunflower SECs—Mechanistic Model*). The model factors in the native sunflower microstructure and assumed correlation factors and can be related to the surface tension driven dissolution of the gas bubbles encapsulated in the SECs. This model was compared with the experimental size of the shrinking air bubbles encapsulated in the SECs, which were measured by analysis of real time CLSM images (**Figure 4**). A representative time evolution of a bubble radius is shown in Figure 4A. Interestingly, in this case, the loading (shrinking air bubble) does not start immediately after submerging the SECs into the BSA solution. Instead there is a lag time before loading takes place. In the representative

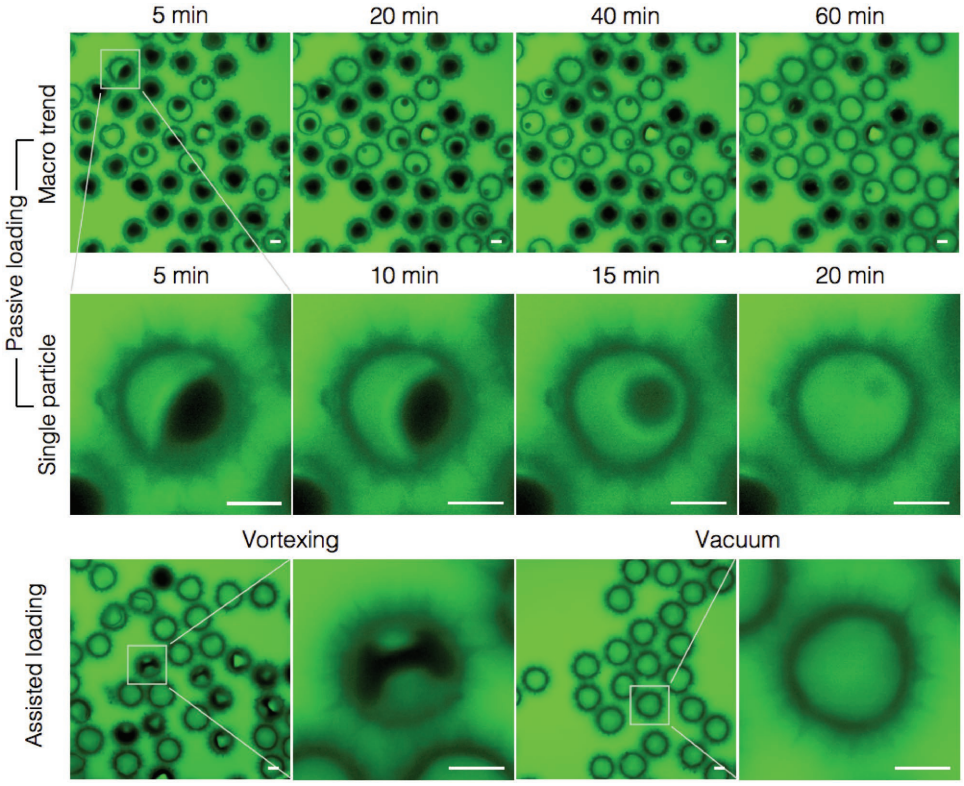

Figure 3. Confocal laser scanning microscopy of BSA-loaded sunflower SECs based on passive and assisted loading. The second row depicts an enlarged view of a representative SEC indicating the evacuation of air from the SEC inner cavity. (Scale bars 10 μm).

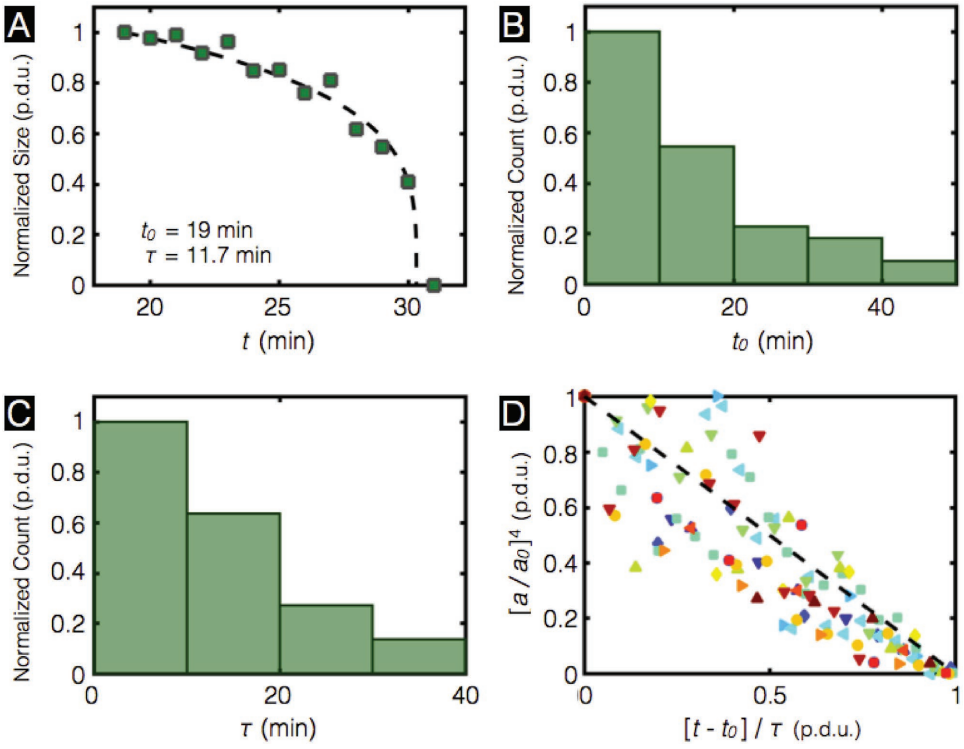

Figure 4. Liquid loading into SECs, measured by tracking encapsulated air bubbles in SECs using confocal microscopy: A) a representative time evolution of a bubble radius; B) a comparative lag time (t_0) distribution for the 45 SECs that showed loading; C) a comparative loading time (τ) distribution for the 45 SECs that showed loading; and D) a comparison of Equation (1) and experimental data for 10 SECs.

bubble dissolution example shown in Figure 4A, the lag time equals t_0 = 19 min and the subsequent loading time equals τ = 11.7 min. The lag time may be caused by the bubble initially blocking the SEC's micron-sized apertures, thus reducing the liquid flow into the SEC. Upon bubble shrinkage, the micron-sized apertures unblock, thus leading to an accelerated liquid flow into the SEC cavity.

Analysis of three sets of 56 confocal microscopy images (5–60 min) presented 91 SECs. Out of these 91 SECs, the loading process was clearly observed for 45 SECs (49%); and for each of those the lag time t_0 and the loading time τ were determined. Calculated mean and standard deviation values were $t_0 = 14 \pm 12$ min and $\tau = 13 \pm 9$ min (Figure 4B,C). Notably, 26 SECs (29%) did not show any loading during the 1 h observation period, while 20 SECs (22%), were already loaded within the 5 min following the submerging in BSA solution before the first microscopy image was taken. These SECs were not included in the analysis.

Next, the experimental data were compared to the fluid transport model, which is derived in Section 4.7. The model assumes that the surface tension pushes the air out of the bubble into the surrounding liquid. Based on the mass balance equation, we derived that the bubble radius decreases in time according to a one fourth power law and then from our experimental observations (Figure 4A) a lag time t_0 was introduced to produce Equation (1)

$$a = a_0\left(1 - \left[\frac{t - t_0}{\tau}\right]\right)^{\frac{1}{4}} \quad (1)$$

In Figure 4D, we compare Equation (1) to experimental data by plotting data for 10 SECs on $[(t - t_0)/\tau,\ (a/a_0)^4]$ coordinates. The data follow a straight line (Equation (1)), which confirms that the model captures the dynamics of liquid loading into SECs, which is a surface tension driven dissolution process.

2.3. Loading Optimization and Analysis

To optimize loading and elucidate the loading distribution of dried compounds within SECs, BSA loading into sunflower SECs was evaluated for three different initial BSA-loading proportions, 23, 37.5, and 54.5 wt%. The loading process involves applying a vacuum to the SEC–BSA suspension leading to a reduction in the internal cavity pressure, which in turn applies a force drawing the BSA solution into the hollow SECs.[26,27]

To evaluate the stability of the SEC morphology following the BSA loading and washing processes, and to ensure that external SEC surfaces were free of residual BSA, SEM analysis of the loaded SECs was performed for all three BSA-loading portions (Figure S7, Supporting Information). All SECs exhibited similar structural and morphological features of well-defined spikes with intact uniform sized SECs. Notably, the sunflower SEC surfaces were free of any residual BSA, indicating the encapsulation of BSA within the SEC inner cavities. To further confirm the stability of the micromeritic properties of BSA-loaded sunflower SECs following BSA loading, DIPA analysis of the SECs before and after loading was conducted (Figure S8, Supporting Information). The analysis of 54.5 wt% BSA-loaded SECs indicated that there were no significant changes in SEC microstructure with respect to diameter, circularity, and aspect ratio. Overall, these data imply that the native microstructure of the sunflower SECs enabled the loading of the model protein within the SECs without disrupting their morphological characteristics.

Table 1. Efficiency of bovine serum albumin encapsulation into SECs.

Sunflower SECs:BSA [mg]	BSA-loading proportions[a)] [wt%]	BSA-loading efficiency [wt%]	BSA encapsulation efficiency [%]
150:45	23.0	9.4 ± 0.7	40.6 ± 2.9
150:90	37.5	15.8 ± 1.9	42.2 ± 4.8
150:180	54.5	22.3 ± 1.5	40.8 ± 2.5

[a)]Loading is based on total initial weight of SECs and BSA. Values represent the mean of three batches (n = 3) with standard deviations.

The loading and encapsulation efficiency for varying BSA proportions are summarized in **Table 1**. The efficiency was significantly enhanced with the increase in the BSA-loading portions; a BSA-loading proportion of 54.5 wt% provided a loading efficiency of 22.3 ± 1.5 wt% ($p < 0.05$), compared with BSA-loading proportions of 23 and 37.5 wt%, which resulted in lower loading efficiencies, at 9.4 ± 0.7 and 15.8 ± 1.9 wt%, respectively.

To quantify and further evaluate the loading process, CLSM images of SECs following FITC–BSA loading were obtained and compared with empty SECs (**Figure 5**; Figures S9 and S10, Supporting Information). The CLSM settings were calibrated to produce no visible SEC autofluorescence emissions in the green spectrum. Empty SECs did not exhibit any green fluorescence, thus confirming empty, clean, intact SECs. SECs following FITC–BSA loading demonstrated an increase in the fluorescence intensity trend with the increase of FITC–BSA-loading proportion (Figure 5A; Figure S10, Supporting Information). To confirm the intracavity loading, CLSM z-stack images (Figure S9, Supporting Information) were used to construct 3D images (Figure 5B), which demonstrated that the green fluorescence originated from the inner cavity and not the SECs surface. Additionally, all loaded SECs, with varying FITC–BSA proportions, exhibited an intact, clean microstructure.

The FITC–BSA volume loading was quantified by the fluorescence intensity per SEC. By normalizing the average fluorescence intensities, with a value of 1 being the particle with the greatest fluorescence intensity value and appearing to be full (Figure S10, Supporting Information), we calculated vol% loading values (Figure 5C). The vol% loading values increase with increases in initial FITC–BSA loading proportion. However, to accurately compare the correlation between vol% loading estimations and BSA-loading efficiency wt% values, it is necessary to convert the BSA-loading efficiency wt% values obtained above to BSA:SEC loading fractions (Figure 5D). There is a close correlation between increases in BSA:SEC loading fractions and vol% loading estimations, which provides validation for the encapsulation and analysis processes.

It is possible to estimate what the theoretical maximum BSA-loading efficiency wt% would be if all SECs were 100% full after loading and washing (100 vol% loading) by comparing our fluorescence intensity vol% loading estimations with BSA:SEC loading fractions. For each of the three sets of loading data, 23,

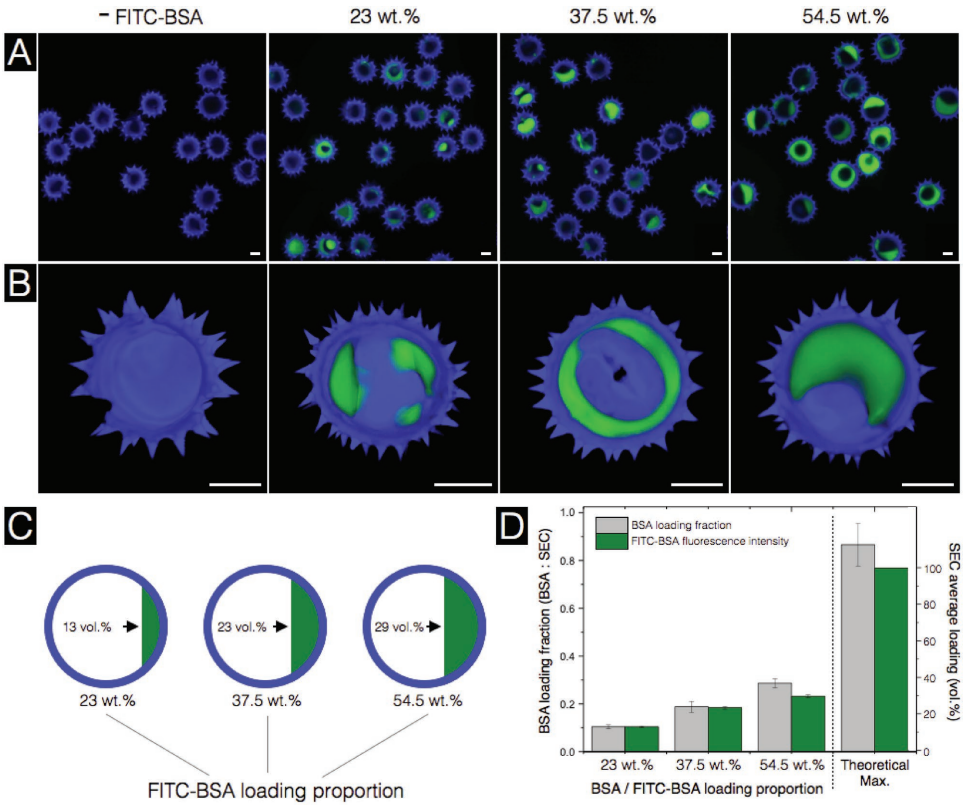

Figure 5. Confocal laser scanning microscopy (CLSM) analysis of FITC–BSA-loaded sunflower SECs: A) unloaded and FITC–BSA-loaded SECs; B) 3D images constructed using z-stacks illustrate the inner cavity of the SECs; C) diagram depicting the average BSA loading based on fluorescence intensity per SEC, vol%; and D) comparative analysis of BSA-loading fraction (BSA:SEC), and SEC average loading, vol%, with estimation of theoretical maximum loading. (Scale bars 10 μm).

37.5, and 54.5 wt%, it is possible to calculate a multiplication factor to determine a theoretical maximum BSA:SEC loading fraction equivalent to 100 vol% loading (Table S3, Supporting Information). Therefore, based on all three sets of data, a theoretical maximum BSA:SEC loading fraction is 0.870 ± 0.089 (Figure 5D), which relates to a theoretical maximum BSA-loading efficiency of 46.4 ± 2.5 wt%. It is important to note that this estimation would require all SECs to be 100 vol% full after loading and washing, which is practically implausible due to some portion of BSA leaching during the washing and handling processes. However, having a robust estimation for the potential maximum loading of SECs provides very useful insight into any future loading optimization work in the field of microencapsulation utilizing SECs or other porous microcapsule systems.

2.4. SEC Protein Release Analysis

Analysis of BSA release from BSA-loaded SECs was analyzed by release studies and CLSM fluorescence intensity analysis (**Figure 6**). A BSA-loading proportion of 54.5 wt% was used based on the loading optimization and analysis conducted in Section 2.3. To investigate the release profile from BSA-loaded SECs, we performed release experiments in pH 1.2 simulated gastric fluid (SGF), and pH 7.4 simulated intestinal fluid (SIF), for up to 60 min (Figure 6A,B). High BSA release rates were observed, of up to 90% in the initial 15 min, and complete release was recorded within 60 min in both SGF and SIF. The observed rapid BSA release is attributed to the passage of molecules through the nanopores and micron-sized apertures in the surface of SECs. A similar release profile was reported from natural sunflower (*H. annuus*) pollen grains and *L. clavatum* SECs in SGF and SIF.[26,27]

For the CLSM fluorescence intensity analysis of FITC–BSA release (Figure 6), it should first be noted that the overall fluorescence intensity observed in SGF (pH 1.2) is less than that observed in SIF (pH 7.4) due to the fluorescence quenching of FITC in acidic conditions.[30] However, by intensity analysis in imageJ, with normalization of the data from 2 to 60 min, it is possible to accurately compare trends within each system. Additionally, the large standard deviations in the inner SEC data are due to significant variations in initial intensity values and are reinforced by differences in rates of release.

The data, for release in SIF (Figure 6A), indicates that the inner SEC fluorescence intensity drops to 49.5 ± 16.8% within 15 min, and 41.6 ± 11.4% within 30 min, relative to 2 min, and remains stable until 60 min. The stabilization of the inner SEC region at ≈40% may be attributed to residual amounts of FITC–BSA remaining in the SECs. The outer SEC fluorescence intensity rises from 12.3 ± 0.9% at 2 min, to 28.7 ± 0.9% at 60 min as FITC–BSA is released into the surrounding media. We assume that the stabilization of inner SEC fluorescence intensity

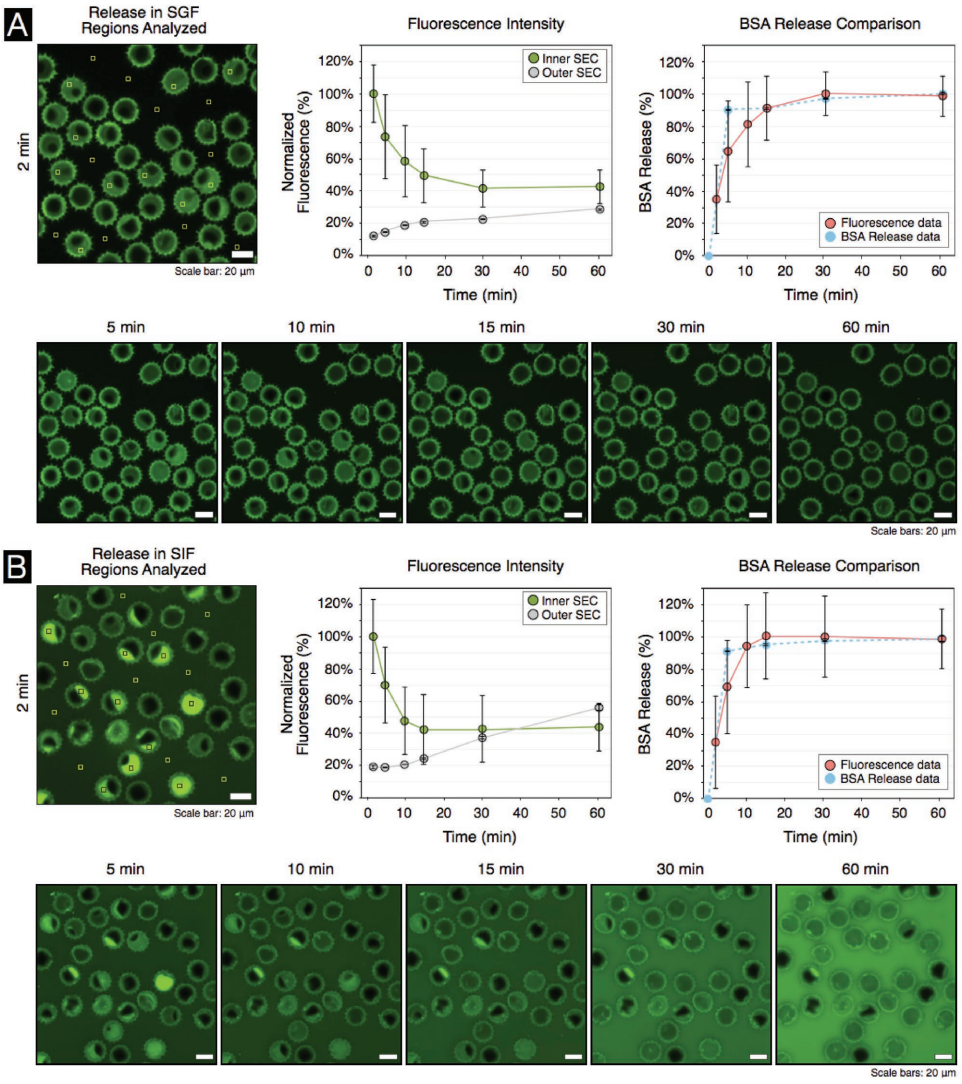

Figure 6. In vitro release of BSA from SECs, comparing BSA release study data and fluorescence intensity analysis data: A) BSA-loaded SECs in simulated gastric fluid, pH 1.2; B) BSA-loaded SECs in simulated intestinal fluid, pH 7.4. BSA release profile data are presented as the average of triplicate measurements with standard deviation ($n = 3$). Fluorescence intensity analysis data is presented as analysis of 10 regions ($n = 10$).

correlates to near complete release of BSA. Comparing the inverse of the inner SEC fluorescence intensity data between 100% and 41.6%, to our BSA release data, over 2–60 min, the trends are shown to be similar. In the 5–10 min region, the fluorescence intensity data indicate slightly slower release than in the BSA release data, however, this may be attributed to the differences in experimental conditions used to collect the data. CLSM analysis comprised a static system at room temperature (≈25 °C); however, BSA release analysis comprised gentle shaking (50 rpm) at 37 °C.

The data, for release in SGF (Figure 6B), indicate that the inner SEC fluorescence intensity drops to 42.3 ± 22.1% within 15 min, relative to 2 min, and remains stable until 60 min. The stabilization of the inner SEC region, also at ≈40%, may be attributed to residual amounts of FITC–BSA remaining in the SECs. The outer SEC fluorescence intensity rises from 19.3 ± 1.2% at 2 min to 55.9 ± 1.9% at 60 min as FITC–BSA is released into the surrounding media. The trends of release based on SEC fluorescence intensity data and the BSA release data, are also similar, wherein subtle variations may be attributed to the differences in experimental conditions.

2.5. Tableted SEC Formulation for Intestinal Protein Release

Oral delivery of therapeutic proteins is still a remaining challenge. In particular, the controlled release of a multiple-units dosage, i.e., microparticle pellets, is attracting growing attention due to having advantages over more common single unit formulations.[31,32] In order to achieve intestinal delivery of the model protein loaded into SECs, the SECs were tableted and enteric coated. The tablets we used for enteric coating contained 149.4 ± 0.3 mg of BSA-loaded SECs, with a consistent tablet diameter (12.92 ± 0.00 mm) and thickness (1.10 ± 0.01 mm)

Table 2. Details of tableted BSA-loaded SECs.

Tableted formulation[a)]	Weight of tablet [mg]	Diameter of tablet [mm]	Thickness of tablet [mm]
Before coat	149.4 ± 0.30	12.92 ± 0.00	1.10 ± 0.01
After coat	169.4 ± 0.85	13.00 ± 0.01	1.49 ± 0.03

[a)]SEC tablets prepared using 13 mm stainless steel press die punch and results represent the mean of three batches ($n = 3$) with standard deviations.

(**Table 2**). To avoid premature release in gastric conditions, the enteric coating was performed using Eudragit L100. Eudragit L100 (EL100) is insoluble under acidic conditions and therefore provides a stable coating within the stomach. Our preliminary exploration of enteric coating indicated that 15% (w/v) EL100 with 15% (w/v) triethyl citrate as a plasticizer provided the most promising formulation for further investigation.

2.5.1. Morphological Analysis of Tableted SECs

To evaluate surface morphology and cross-sectional topography of tableted SECs, SEM images were obtained before and after the coating process (**Figure 7**). The surface roughness of the tableted SECs is the result of the intact and robust SEC microstructure after compression (Figure 7A). The cross-sectional SEM image revealed an intact SEC microstructure with native spike morphology, without any breakages; this implied that SECs were present as discrete particles in the tablet (Figure 7B). Moreover, although compressed, the fundamental SEC architecture was retained even following compression, without any pharma excipients, indicating the robust microstructure of sunflower SECs.

Analysis of tablet morphology and SEC particle counts provides further insight into the tableted SEC structure. Dynamic image particle analysis (DIPA) measurements indicate $1.83 \pm 0.17 \times 10^5$ SECs per milligram. A BSA-loaded SEC loading efficiency of 22.3% results in 116.6 mg of SECs per 150 mg tablet, correlating to 2.14×10^7 SECs per tablet. With a precoating tablet volume of 1.44×10^{11} μm^3, each SEC comprises 6.75×10^3 μm^3, and based on a compressed SEC diameter of 30.0 μm (Figure 7A), the thickness estimation of a compressed SEC is 9.6 μm. Therefore, each 150 mg tablet comprises ≈430.7 SECs across the tablet diameter, and 115.1 SECs across the tablet thickness. Regarding BSA distribution throughout the tablet,

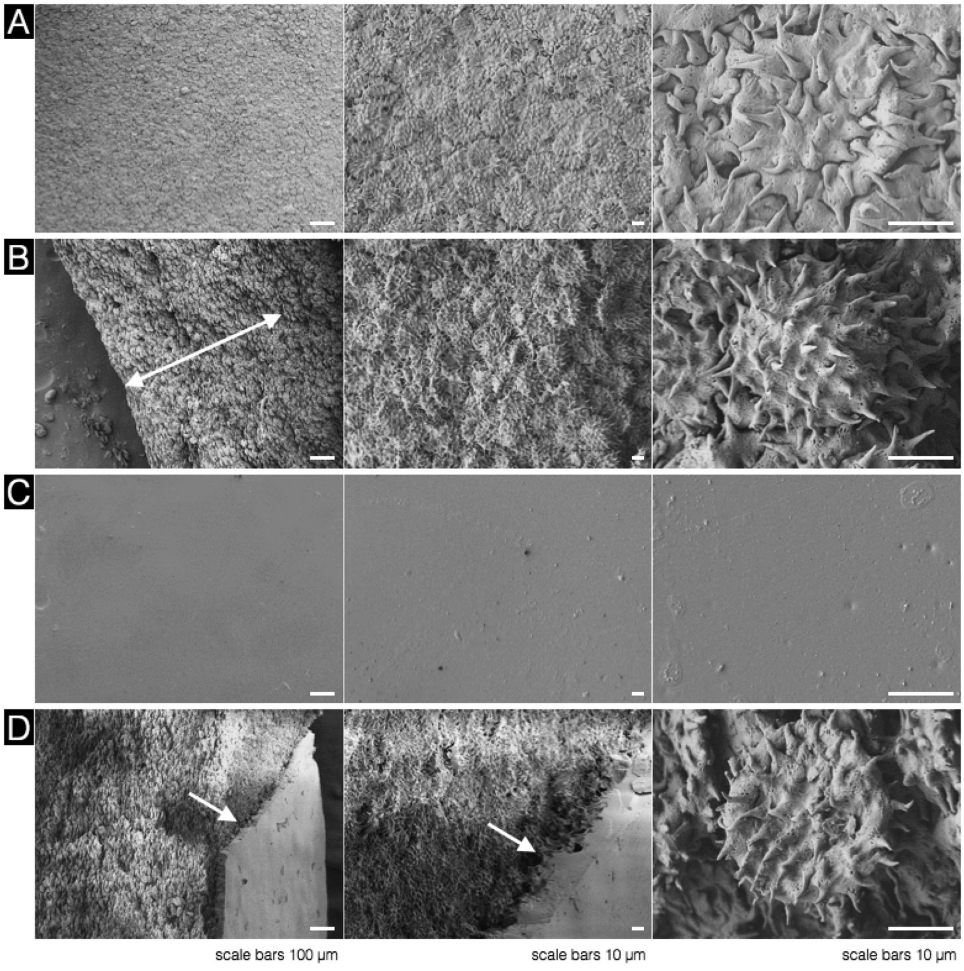

Figure 7. Scanning electron microscopy images of tableted BSA-loaded SECs with and without 15% (w/v) Eudragit L100: A) surface prior to enteric coating; B) cross-section prior to enteric coating, arrow indicates the cross-sectional direction; C) surface following enteric coating; and D) cross-section following enteric coating, arrows indicate the enteric coating layer.

we may assume a uniform distribution with an average SEC volume loading of 29%, correlating to an SEC loading efficiency of 22.3% (Figure 5; Figure S10, Supporting Information).

Following the enteric coating, the surface of the tableted SECs was smoother (Figure 7C), compared with tableted SECs only (Figure 7A), thus implying the formation of a continuous protective layer. The cross-sectional image of enteric coated tableted SECs confirmed the formation of a 40–50 µm coating layer on the surface of the SECs (Figure 7D). Overall, the morphological analysis of the tablets confirmed the presence of intact BSA-loaded SECs, and a well-defined layer of enteric coating.

2.5.2. Analysis and Optimization of Controlled Release

It is crucial for intestinal targeted delivery of proteins to ensure that the protein is not exposed to harsh gastric conditions. The release profile of the tableted BSA-loaded SECs following the enteric coating was measured in vitro in SGF and SIF (**Figure 8**). The release profile exhibited a controlled release of the protein, with no release in SGF for up to 2 h, and a complete release in SIF, 100%, within 8 h. These data indicate the suitability of our tablet formulation to protect encapsulated proteins in gastric conditions and to target a significant portion of the intestinal area.[13,14]

Release control studies were conducted with enteric coated tablets with no SECs, as well as with BSA-loaded SEC tablets without enteric coating (Figure 8), and further control tablet details are provided in Table S4 (Supporting Information). The enteric coated tablets with no SECs utilized Eudragit L100 as a dry matrix[33] and contained the same proportion of BSA as in our study tablets. The results indicate that the tablets are stable up to 6 h, 2 h in SGF + 4 h in SIF, with 2.6 ± 1.2% release. Then, after 8 h in SIF we see a total BSA release of 31.3 ± 1.9%. However, even at 30 h, there is only 54.2 ± 9.7% release, suggesting that this system is suboptimal for targeted intestinal delivery. The BSA-loaded SEC tablets without enteric coating exhibit 39.9 ± 19.1% in 2 h in SGF and a total of 92.8 ± 15.6% with an additional 1 h in SIF, suggesting that this system is unstable and not appropriate for targeted intestinal delivery.

The observed extended release profile of the BSA-loaded SEC enteric coated tablets in SIF conditions is attributed to tablet fragmentation into compact aggregates of SECs. We propose that as the enteric coating slowly erodes, the SEC tablet starts disintegrating as larger compact aggregates of BSA-loaded SECs. Hence, our tableted SEC formulations are expected to spread uniformly throughout the gastrointestinal tract (GIT), thereby avoiding the rapid release of a therapeutic protein or drugs at a single location. Distributed release of multiple smaller units in the GIT helps reduce the potential of drug toxicity and also results in more uniform absorption. In order to investigate the microstructural changes of tableted SECs after in vitro release, we performed SEM analysis. The SEM analysis (Figure S11, Supporting Information) indicated discrete microparticles with intact surface topography and structure similar to native SECs, confirming the robust nature of sunflower SECs and highlighting their potential for use as a microparticle-based delivery system.

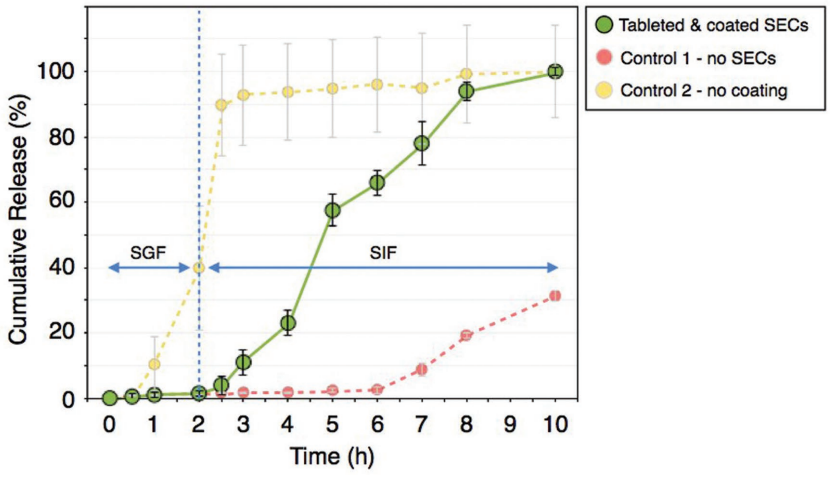

Figure 8. In vitro release of BSA from enteric-coated SEC tablets and controls. Tablet release profiles are based on incubation of 2 h in simulated gastric fluid, pH 1.2, and 8 h in simulated intestinal fluid, pH 7.4. Data are presented as the average of triplicate measurements with standard deviation ($n = 3$).

3. Conclusion

SECs provide a highly compelling platform for microencapsulation and drug delivery, particularly for the oral administration of therapeutic proteins. We have successfully developed an effective and low-cost controlled delivery system for proteins. SEC extraction from Sunflower (*H. annuus*) pollen grains was optimized and achieved with reduced duration processing. The SECs displayed a highly monodisperse size distribution, mechanical robustness, and the ability to encapsulate the model protein with high efficiency.

The vacuum-loading BSA encapsulation and SEC tableting methods utilized are straightforward mechanical processes, which do not require the use of additional reagents, organic solvents, or high shear forces, which can damage proteins. Additionally, this study demonstrated insights into protein loading mechanisms through real time and post processing CLSM observations of FITC–BSA-loaded SECs. For the first time, a detailed investigation of protein loading and distribution in BSA-loaded SEC batches was revealed with the assistance of CLSM and mathematical modeling. The validity of these observations was supported by a high correlation between CLSM fluorescence intensity analysis and experimental quantification of BSA loading. It was shown that the evacuation of air from SEC internal cavities through SEC surface nanopores and micron-sized apertures drives the BSA-loading process. Additionally, these studies have led to a robust estimation of the maximum potential loading of these SECs, therefore providing a useful indicator of practical loading efficacy

in this and future studies utilizing SECs or other porous microcapsule systems.

Finally, the tableting of BSA-loaded SECs and enteric coating using Eudragit L100 produced stable multiparticulate tablets for oral delivery. The enteric coated tablets exhibited successful inhibition of BSA release in simulated gastric fluid for 2 h and allowed for complete release within 8 h in SIF. The SECs size and microstructure were preserved throughout the loading, tableting, and release processes. These results taken together imply that the SECs may protect the encapsulated protein up to its release at the targeted site. Furthermore, the SECs ability to retain their morphology and porosity, following tableting and in vitro release, provides the benefit of a unified rapid release of the protein from the SECs upon tablet disintegration at the desired site. The release profile was modulated with polymers, thus also highlighting the potential flexibility of SECs as a delivery system. To conclude, we have demonstrated that SECs provide an effective and versatile drug formulation platform enabling intestinal targeted release of orally delivered protein therapeutics.

4. Experimental Section

Materials: BSA, FITC-conjugated BSA, phosphoric acid (85% w/v), hydrochloric acid, potassium hydroxide, sodium hydroxide, ethanol, and acetone were purchased from Sigma-Aldrich (Singapore). Defatted sunflower (*Helianthus annuus L.*) pollen grains were purchased from Greer Labs (NC, USA). Vectashield (H-1000) was purchased from Vector labs (CA, USA). Sticky-slides, D 263 M Schott glass, No.1.5H (170 µm, 25 mm × 75 mm) unsterile were purchased from Ibidi GmbH (Munich, Germany). Milli-Q water was used in all experiments. Eudragit L100 was purchased from Evonik Industries (Essen, Germany). Perfluoroalkoxy polymer flasks were purchased from Vitlab (Grossostheim, Germany). A stainless steel pellet press die (13 mm) was purchased from Specac (Kent, UK).

Isolation of Sunflower Sporopollenin Exine Capsules: The sunflower SECs were extracted as described elsewhere.[28] Briefly, pollen grains underwent acidolysis in phosphoric acid for various durations (1, 5, 10, 20 h). The SECs were then collected by vacuum filtration and washed extensively in warm solvents, bases, and acids, and then dried until stable weight.

Elemental Analysis: Elemental analysis of defatted sunflower pollen grains and SECs was performed as described elsewhere.[28] Briefly, samples were dried until stable weight and measurements were performed in triplicate. Protein content was calculated based on percent nitrogen with a multiplication factor of 6.25.[7,28] Normalized protein removal values were calculated relative to the maximum amount of protein, which can be removed using our SEC extraction protocol.

Mass Spectrometry Analysis: MALDI-TOF mass spectrometry was performed with ground and ethanol extracted pollen and SECs. 5 mg of pollen or SECs was ground with a mortar and pestle, then suspended in 0.5 mL of ethanol, followed by vortexing for 2 min. 0.7 µL of the suspension was added to a MALDI plate followed by addition of 1 µL of an α-cyano-4-hydroxycinnamic acid matrix solution. After drying, samples were analyzed in a Shimadzu Biotech Axima Performance MALDI-TOF system, in linear mode, with a power of 90, and 100 profiles per run. All samples were run in triplicate and data were processed with Gaussian smoothing (100), and baselined (100).

Dynamic Image Particle Analysis: Dynamic image particle analysis was performed as described elsewhere.[28] Briefly, the system was setup with a 200 µm flow cell and a 20× lens. Water-based solutions were prepared with a sample concentration of 2 mg mL^{-1}. Analysis was performed on 1000 well-focused particles and all measurements were recorded in triplicate. Data were plotted as spline curves fitted to histogram data for ease of comparison.

Confocal Laser Scanning Microscopy Analysis: Fluorescence microscopy analysis was performed as described elsewhere.[28] Briefly, samples were mounted between slides with vecta shield. Imaging was performed successively with three laser excitation channels: 405, 488, and 561 nm, with three respective emission filters: 416–477, 498–550, 572–620 nm. A 63× oil or 20× regular objective lense was used for imaging. At least three images were captured per sample.

For fluorescence intensity analysis of FITC–BSA loading into SECs, green channel CLSM images were used from the mid region of the SECs. Only whole SECs were utilized for fluorescence analysis. The total fluorescence intensity values for the first 50 SECs of each sample set were selected, i.e., FITC–BSA-loading proportions of 23, 37.5, and 54 wt%. The SEC fluorescence intensity values for all 150 SECs were normalized, with 1.0 being the highest value out of all 150 SECs. The normalized SEC fluorescence data were used for further statistical analysis and sample set comparisons. Assuming that an SEC with a normalized fluorescence intensity value of 1.0 is equivalent to having a loading of 100 vol%, then the average SEC fluorescence intensity values of each sample set can be correlated to an equivalent loading vol% estimation.

Surface Morphology Evaluation by Scanning Electron Microscopy: SEM imaging was performed as described elsewhere.[28] Briefly, samples were coated with platinum at 20 mA, 60 s, and images were obtained with an acceleration voltage of 5.00 kV at various magnifications.

BSA Loading into Sunflower SECs—Mechanistic Model: The BSA loading into SECs (radius a_0, thickness d, and porosity ε) is modeled by considering the dissolution of the air bubble inside the SEC (bubble radius a and volume $V = 4/3\pi a^3$). The model is based on well-established concepts in fluid mechanics, and extensive treatments of these principles have been reported.[34–36]

The change of the bubble volume in time is governed by the mass balance equation

$$c\frac{\mathrm{d}V}{\mathrm{d}t} = -\varepsilon A_0 J \tag{2}$$

where $c = p_\infty/RT$ is the air mass density inside the bubble, R is the universal gas constant, T is the temperature, $p_\infty = 10^5$ kg m^{-1}s^{-2} is the ambient pressure, $A_0 = 4\pi a_0^2$ is the inner surface area of the capsule, and J is the air diffusive mass flux in solution, whose resistance is assumed to be concentrated over the SEC shell

$$J = \frac{D}{d}(c_0 - c_\infty) \tag{3}$$

Here D is the diffusivity of the air in the liquid, $c_0 = p_0/RTk_\mathrm{H}$ is the saturated air mass density in the liquid at the air–liquid interface, $c_\infty = p_\infty/RTk_\mathrm{H}$ is the saturated air mass density in the liquid outside the capsule, k_H is the Henry constant, and $p_0 = p_\infty + \Delta p$ is the pressure inside the bubble, where the difference to the pressure outside the bubble is due to the gas–liquid surface tension, σ, according to Laplace's law

$$\Delta p = \frac{2\sigma}{a} \tag{4}$$

Noting that $\mathrm{d}V/\mathrm{d}t$ is negative and combining all relations, we arrive at the following equation for the change of the radius of the dissolving gas bubble

$$\frac{\mathrm{d}a}{\mathrm{d}t} = -\frac{\sigma\varepsilon A_0 D}{2\pi d a^3 p_\infty k_\mathrm{H}} \tag{5}$$

which is solved by

$$a = a_0\left(1 - \left[\frac{t}{\tau}\right]\right)^{\frac{1}{4}} \tag{6}$$

where the dissolution time scale is given by

$$\tau = \frac{da_0^2 p_\infty k_H}{8\sigma\varepsilon D} \quad (7)$$

Equations (6) and (7) provide the rate of liquid loading into the SECs, where it has been recognized that the loading is equivalent to the dissolution of the encapsulated gas bubbles. The model assumes that the dissolution is driven by surface tension, which pushes the air out of the bubble into the surrounding liquid. Although we do not know all material constants, which are involved in Equation (7), we have qualitatively compared Equation (6) to experimental BSA-loading data. In Figure 4D above, we show that the measured radii of encapsulated gas bubbles follow a one-fourth power law, as predicted by Equation (6), which validates the proposed mechanism of liquid loading in the SECs, as a surface-tension-driven dissolution process.

Bovine Serum Albumin Encapsulation into Sunflower SECs: BSA loading into sunflower SECs was performed using a vacuum loading technique.[27] 150 mg of SECs was suspended in 1.2 mL of aqueous BSA solution at one of three different BSA-loading proportions (23, 37.5, 54.5 wt%) in polypropylene tubes to form a homogeneous suspension and then mixed for 10 min using a vortex mixer (IKA, Staufen, Germany). The samples were then lyophilized for 12 h. The tubes were collected and the loaded SECs were washed using 2 mL water then centrifuged to remove residual BSA, this washing step was repeated for a total of two washes. The BSA-loaded SECs were frozen at −80 °C for 30 min and lyophilized for 24 h. The resultant sunflower SECs were stored at −20 °C. Placebo SECs were prepared and stored following the same procedure. In order to determine the localization of BSA within the sunflower SECs, FITC-conjugated BSA was encapsulated in SECs using the same procedure as the above-mentioned vacuum loading technique.

Encapsulation Efficiency: Five mg of BSA-loaded SECs were added to 1.4 mL of phosphate buffered saline (PBS), vortexed for 5 min, and then probe sonicated for three cycles of 10 s (40% amplitude).[27] The extracted BSA was collected by passing the solution through a 0.45 µm PES syringe filter (Agilent, CA, USA) with the BSA extraction step repeated for a total of two times. The absorbance values were measured at 280 nm (Boeco-S220, Germany) using a placebo extract as a blank and the BSA in the SECs was quantified using a BSA standard curve.

Tableting and Enteric Coating: Three kinds of tablets were prepared. (1) Tablets comprising BSA-loaded sunflower SECs (150 mg per tablet) with a BSA-loading proportion of 54.5 wt%, which were tableted and enteric coated. (2) Control tablets with no SECs, comprising a dry mix of 33 mg of BSA and 117 mg of Eudragit-L 100, equivalent to a BSA-loading efficiency of 22.3% as used in the BSA-loaded sunflower SEC tablets. Wherein, the BSA and Eudragit were first passed through a 50 µm sieve to ensure uniformity and vortexed together for 5 min to blend, then 150 mg of the blend was tableted and enteric coated. (3) Control tablets comprising BSA-loaded sunflower SECs (150 mg per tablet) with a BSA-loading proportion of 54.5 wt%, which were tableted and not enteric coated. For tableting, either 150 mg of BSA-loaded sunflower SECs (150 mg per tablet), or 150 mg of the BSA/Eudragit dry mix, were loaded in a 13 mm pellet press then compressed with a 5 ton load for 20 s (cross-sectional area of 132.75 mm^2 with compression pressure of 370 MPa). For enteric coating, tablets were dip-coated in a solution of 15% (w/v) Eudragit-L 100 in a mixture of isopropyl alcohol:acetone (92:8, v/v) with triethyl citrate as a plasticizer (15%, w/v). Dipping duration was 5 s followed by drying at room temperature. This coating step was repeated for a total of three coatings and followed by drying under vacuum for 2 h at room temperature. The dimensions of the tablets were recorded before and after tableting.

In Vitro Drug Release in Simulated Gastric Fluid and Simulated Intestinal Fluid: In vitro release of BSA from sunflower SECs was performed by suspending 5 mg of BSA-loaded SECs in 1.4 mL of pH 1.2 SGF (0.1 M HCl) or SIF (PBS, pH 7.4).[27] The mixture was incubated in an orbital shaker incubator (LM-450D, Yihder, Taiwan) at 37 °C at 50 rpm. Supernatants were collected at various time intervals by centrifugation of samples at 9391 rcf (10 000 rpm) for 30 s, whereupon fresh release media were added to the samples. Supernatants were filtered using PES filters. Absorbance values were measured at 280 nm using a placebo extract as a blank and the released BSA was quantified using a BSA standard curve. To simulate gastrointestinal conditions in the case of the tablets, the BSA release was performed for 2 h in SGF followed by 8 h in SIF. The tablets were added to 20 mL of release media then incubated at 37 °C at 50 rpm in an orbital shaker incubator. At various time points, 1 mL of release media was collected followed by the addition of fresh release media. The released BSA was quantified as described above.

Statistical Analysis: Statistical analysis of data was performed based on two-tailed *t*-tests, with $P < 0.05$ being considered to be statistically significant. Quantitative data from loading and in vitro release are reported as mean values ± standard deviation of three separate measurements.

Supporting Information

Supporting Information is available from the Wiley Online Library or from the author.

Acknowledgements

This work was supported by the Competitive Research Programme (NRF-CRP10-2012-07) of the National Research Foundation of Singapore (NRF), and by the Creative Materials Discovery Program through the National Research Foundation of Korea (NRF) funded by the Ministry of Science, ICT, and Future Planning (2016M3D1A1024098). Also, the research was aided by a Start-Up Grant (SUG) from Nanyang Technological University (M4080751.070). Thanks to Dr. Thresen Mathew (NTU, MSE) for assistance with MALDI-TOF analysis.

Conflict of Interest

The authors declare no conflict of interest.

Keywords

oral delivery, protein delivery, sporopollenin exine capsules (SECs), sunflower pollen, targeted intestinal delivery

Received: January 17, 2017
Revised: April 13, 2017
Published online: June 7, 2017

[1] S. Mitragotri, P. A. Burke, R. Langer, *Nat. Rev. Drug Discovery* **2014**, *13*, 655.
[2] A. N. Zelikin, C. Ehrhardt, A. M. Healy, *Nat. Chem.* **2016**, *8*, 997.
[3] R. C. Mundargi, M. G. Potroz, J. H. Park, J. Seo, E.-L. Tan, J. H. Lee, N.-J. Cho, *Sci. Rep.* **2016**, *6*, 19960.
[4] A. Diego-Taboada, S. T. Beckett, S. L. Atkin, G. Mackenzie, *Pharmaceutics* **2014**, *6*, 80.
[5] S. Barrier, A. Diego-Taboada, M. J. Thomasson, L. Madden, J. C. Pointon, J. D. Wadhawan, S. T. Beckett, S. L. Atkin, G. Mackenzie, *J. Mater. Chem.* **2011**, *21*, 975.
[6] S. Barrier, A. S. Rigby, A. Diego-Taboada, M. J. Thomasson, G. Mackenzie, S. L. Atkin, *LWT-Food Sci. Technol.* **2010**, *43*, 73.
[7] S. U. Atwe, Y. Ma, H. S. Gill, *J. Controlled Release* **2014**, *194*, 45.
[8] A. Diego-Taboada, L. Maillet, J. H. Banoub, M. Lorch, A. S. Rigby, A. N. Boa, S. L. Atkin, G. Mackenzie, *J. Mater. Chem. B* **2013**, *1*, 707.

[9] M. Lorch, M. J. Thomasson, A. Diego-Taboada, S. Barrier, S. L. Atkin, G. Mackenzie, S. J. Archibald, *Chem. Commun.* **2009**, 6442.
[10] H. Ma, P. Zhang, J. Wang, X. Xu, H. Zhang, Z. Zhang, Y. Zhang, Y. Ning, *J. Microencapsulation* **2014**, *31*, 667.
[11] A. Diego-Taboada, P. Cousson, E. Raynaud, Y. Huang, M. Lorch, B. P. Binks, Y. Queneau, A. N. Boa, S. L. Atkin, S. T. Beckett, G. Mackenzie, *J. Mater. Chem.* **2012**, *22*, 9767.
[12] A. Wakil, G. Mackenzie, A. Diego-Taboada, J. G. Bell, S. L. Atkin, *Lipids* **2010**, *45*, 645.
[13] M. Koziolek, M. Grimm, F. Schneider, P. Jedamzik, M. Sager, J.-P. Kühn, W. Siegmund, W. Weitschies, *Adv. Drug Delivery Rev.* **2016**, *101*, 75.
[14] V. K. Pawar, J. G. Meher, Y. Singh, M. Chaurasia, B. S. Reddy, M. K. Chourasia, *J. Controlled Release* **2014**, *196*, 168.
[15] B. Leader, Q. J. Baca, D. E. Golan, *Nat. Rev. Drug Discovery* **2008**, *7*, 21.
[16] M. C. Koetting, J. F. Guido, M. Gupta, A. Zhang, N. A. Peppas, *J. Controlled Release* **2016**, *221*, 18.
[17] A. Mullard, *Nat. Rev. Drug Discovery* **2013**, *12*, 87.
[18] E. Moroz, S. Matoori, J.-C. Leroux, *Adv. Drug Delivery Rev.* **2016**, *101*, 108.
[19] S. Gupta, A. Jain, M. Chakraborty, J. K. Sahni, J. Ali, S. Dang, *Drug Delivery* **2013**, *20*, 237.
[20] M. Morishita, N. A. Peppas, *Drug Discovery Today* **2006**, *11*, 905.
[21] M. Koziolek, G. Garbacz, M. Neumann, W. Weitschies, *Mol. Pharm.* **2013**, *10*, 2211.
[22] J. Renukuntla, A. D. Vadlapudi, A. Patel, S. H. Boddu, A. K. Mitra, *Int. J. Pharm.* **2013**, *447*, 75.
[23] M. J. M. Villena, F. Lara-Villoslada, M. A. R. Martinez, M. E. M. Hernandez, *Int. J. Pharm.* **2015**, *487*, 314.
[24] R. C. Mundargi, V. R. Babu, V. Rangaswamy, P. Patel, T. M. Aminabhavi, *J. Controlled Release* **2008**, *125*, 193.
[25] R. C. Mundargi, V. Rangaswamy, T. M. Aminabhavi, *Drug Dev. Ind. Pharm.* **2011**, *37*, 977.
[26] R. C. Mundargi, M. G. Potroz, S. Park, J. H. Park, H. Shirahama, J. H. Lee, J. Seo, N. J. Cho, *Adv. Funct. Mater.* **2016**, *26*, 487.
[27] R. C. Mundargi, M. G. Potroz, S. Park, H. Shirahama, J. H. Lee, J. Seo, N. J. Cho, *Small* **2016**, *12*, 1167.
[28] R. C. Mundargi, M. G. Potroz, J. H. Park, J. Seo, J. H. Lee, N.-J. Cho, *RSC Adv.* **2016**, *6*, 16533.
[29] Y. Hou, Z. Wu, Z. Dai, G. Wang, G. Wu, *J. Anim. Sci. Biotechnol.* **2017**, *8*, 24.
[30] C. J. Breen, M. Raverdeau, H. P. Voorheis, *Sci. Rep.* **2016**, *6*, 25769.
[31] A. Kambayashi, H. Blume, J. B. Dressman, *Eur. J. Pharm. Biopharm.* **2014**, *87*, 236.
[32] A. Maltais, G. E. Remondetto, M. Subirade, *Food Hydrocolloids* **2010**, *24*, 518.
[33] J. Grund, M. Koerber, M. Walther, R. Bodmeier, *Int. J. Pharm.* **2014**, *469*, 94.
[34] R. B. Bird, W. E. Stewart, E. N. Lightfoot, *Transport Phenomena*, Wiley, New York **2007**.
[35] P.-G. de Gennes, F. Brochard-Wyart, D. Quere, *Capillarity and Wetting Phenomena*, Springer-Verlag, New York **2004**.
[36] V. G. Levich, *Physicochemical Hydrodynamics*, Prentice-Hall, Englewood Cliffs, NJ **1962**.